ELSEVIER

Journal of Photochemistry and Photobiology A: Chemistry 146 (2002) 175–188

Journal of Photochemistry and Photobiology A:Chemistry

www.elsevier.com/locate/jphotochem

Photoelectrochemical characterization of nanocrystalline TiO_2 films on titanium substrates

Fabiana Y. Oliva [a], Lucía B. Avalle [a,*], Elizabeth Santos [b], Osvaldo R. Cámara [a]

[a] *INFIQC Departamento de Fisicoquímica, Facultad de Ciencias Químicas, Universidad Nacional de Cordoba, Ciudad Universitaria, 5000 Cordoba, Argentina*

[b] *Facultad de Matemática Astronomía y Física, Universidad Nacional de Cordoba, Ciudad Universitaria, 5000 Cordoba, Argentina*

Received 9 October 2001; received in revised form 11 October 2001; accepted 16 October 2001

Abstract

This paper deals with the photo-electrochemical characterization of nanocrystalline TiO_2 films deposited on titanium substrates in 0.1 M NaCl solutions. These films were confirmed to contain mainly anatase crystallites by X-ray diffraction (XRD) and have n-type properties by UV-photoelectron spectroscopy (UPS). Experiments were also performed on thermal and electrochemical TiO_2 oxides formed in air or the same electrolyte, respectively, to delineate the role in the electrochemical behavior of the nanocrystalline films and differentiate their properties from the titanium substrate and its spontaneously formed oxide. Systematic enhancement of the photocurrent was observed for nanocrystalline TiO_2 films compared with the thermal oxide. This effect arises principally from the area factor but, as it was observed by UPS, capacitance and cyclic voltammetry measurements, it was not the only factor affecting the photocurrent response. It was found that the shape of the photocurrent vs. wavelength curves depend on the electrode potential when the electrode is irradiated at energies above the optical bandgap of the films (3.2 eV for anatase single crystal), whereas at energies below the bandgap, it remains almost potential independent. The capacitance measurements of the nanocrystalline Ti/TiO_2 electrodes in the dark and under illumination conditions did not show substantial changes under our experimental conditions. This fact is indicating the pinning of semiconductor bands still during illumination. The origin of this effect was related with a high rate of surface trap filling. The absorption coefficient for nanocrystalline oxide films was calculated from i_{ph}^2 vs. V plots and a value of $1 \times 10^2\ cm^{-1}$ was obtained. The flat band potential (V_{FB}) calculated from photocurrent plots was not in good correlation with the Nernstian behavior obtained from impedance measurements (Mott–Schottky plots).

Keywords: Sub-bandgap absorption; TiO_2 nanocrystalline; Thermal oxide; Capacitance measurements; Cyclic voltammetry

1. Introduction

Previous studies [1] about the electrochemical behavior of the nanocrystalline TiO_2 films and their interaction with macromolecules of biological interest have suggested an important role of the surface and bulk characteristics of the electrodeposited TiO_2 thin films in determining the response of the semiconductor film/electrolyte interface. The behavior of nanocrystalline films is often different from that of compact semiconductor electrodes. Grätzel and co-workers [2] have interpreted the photoeffects observed with these electrodes in terms of an array of weakly coupled colloidal particles. This means that no space charge layer can be formed in the porous films due to the small size of the TiO_2 particles and the almost inexistent Ti(III) species, both facts conferring their insulating character. However, the photoelectrochemical behavior of electrodeposited nanocrystalline films depends strongly on the experimental and chemical environmental conditions that are present in the synthesis procedure [3,4]. Therefore, the practical importance of the oxide thin film photo-characterization lies not only in the knowledge of the electrical and optical properties of its surface, but also of the bulk of the materials. Grätzel and co-workers [2] have interpreted the change of capacity during bandgap excitation of the TiO_2 film in terms of trapping of photogenerated holes in surface states that lead to unpinning of the energy bands. Our previous studies [1] show that the dependence of the capacity, under dark conditions, on the potential and pH can be associated with the generation of surface states on TiO_2 due to protein–substrate interactions. The study of these films under illumination should provide further information for adsorption processes at a given substrate [1] and for photodegradation processes [5]. These films have proved to be useful for these before mainly because they have a high surface area in contact with the electrolyte.

* Corresponding author. Fax: +54-351-4334188.
E-mail address: luciaavalle@yahoo.com (L.B. Avalle).

1010-6030/02/$ – see front matter
PII: S1010-6030(01)00614-1

This paper reports on the characterization of nanocrystalline TiO_2 film electrodeposited on titanium substrates using UV-phototelectron spectroscopy (UPS), X-ray difraction analysis (XRD), cyclic voltammetry, capacitance and photoelectrochemical measurements. These experiments provided information on the electronic properties of the TiO_2 films in the dark and during illumination. The photocurrent dependence on electrode potential and solution pH was also investigated. Supra-bandgap and sub-bandgap photocurrent generation were determined and a physical model is proposed taking into account the photocurrent dependence on light energy and electrode potential. The results of numerical simulations in order to fit the experimental photocurrent vs. photon energy and/or potential curves are presented according to different models.

2. Experimental

2.1. Materials

2.1.1. Chemicals

The measurements were performed in 0.1 M NaCl aqueous solutions. The pH of the solution was adjusted either with concentrated HCl or NaOH solutions before each experiment and checked with an Orion 960 autochemistry system with a glass electrode (Orion BN 9104). Despite the fact that this solution is not a buffer, no significant variations in the solution pH were observed during the experiment. The pH of the solution was varied between 3.0 and 10.0. All the solutions were prepared with purified water from Milli-Q, Millipore system. All chemicals were of analytical grade, purchased from Merck, and used without further purification.

2.1.2. Cells and electrodes

A three-electrode cell system was used for all the electrochemical experiments carried out at room temperature. Before the measurements, the electrolytes were purged with N_2 for at least 30 min to remove dissolved oxygen. The counter electrode was a platinum foil electrode with large area and the reference electrode was a KCl saturated Ag/AgCl electrode to which all potentials in the text will be referred.

A titanium disc from John Matthey Electronics (99.7% purity) was employed as substrate for the preparation of the different Ti/TiO_2 working electrodes with only one face exposed to solution (1 cm^2 area). This substrate was mechanically polished with different abrasive papers and finally with 1 μm alumina, then chemically etched by immersion in a $HF:HNO_3:H_2O$ (1:4:5 in volume) solution for 10 s. Thin TiO_2 nanocrystalline films were prepared as described previously [6] on the substrates by cathodic electrodeposition in TiO^{2+}–HNO_3 solution. The electrodeposition process was carried out potentiostatically at −1.2 V for 5 min. After that the obtained Ti(IV) hydrous-oxide coating was dried in air at room temperature. This process was performed several times (up to 10 times) in order to obtain films of different thickness. Finally, the electrode with the hydrous-oxide film was thermally treated at temperature around 400 °C in air atmosphere. This procedure allows to obtain a film thickness of about 0.5 μm for 10 deposition stages. The SEM studies showed the film to be porous and the roughness factor was determined to be 450 [1].

Besides the nanocrystalline TiO_2 films, the electrochemical and photoelectrochemical experimental methodologies were also performed on TiO_2 electrodes prepared thermally and electrochemically. The same titanium disc substrate was employed for the three types of oxide films in order to obtain real comparative results. The electrochemical oxide film was obtained by cycling the titanium electrode in 0.1 M NaCl solution in the potential range between −1.0 and 1.5 V vs. Ag/AgCl at 100 mV s^{-1}, up to a stabilized *i–V* profile. The thermal oxide film was prepared by heating the titanium substrate at 400 °C in air for 1 h. In both cases, the substrate was previously treated in the same way as for the nanocrystalline film.

2.2. Methods

2.2.1. UPS and XRD measurements

UPS measurements were performed only on nanocrystalline TiO_2 films at the Campinas Sincrotron, SP, Brazil in the toroidal grating monochromator (TGM) beam line. The pressure in the sample chamber was in the 10^{-9} mbar range. In order to obtain information about the composition at different film depths, TiO_2 samples were argon sputter etched (2 KeV, 20 μA) in the preparation chamber for different periods of time.

XRD spectra were obtained between 20 and 60 2θ degrees using a Rigaku (Miniflex) equipment.

2.2.2. Cyclic voltammetry measurements

Voltammetric curves were obtained with the three different oxide film electrodes after stabilization by cycling between −1.0 and 1.5 V vs. Ag/AgCl (five cycles) using different potential sweep rates (20 and 100 mV s^{-1}) and solution pH values (3.0–10.0 range). The electrochemical instrumentation was a ZANHER IM5D analyzer with a potentiostat—wave generator module. In all cases, the potential scan direction started from the electrode rest potential at open circuit (ca. −0.185 V) towards more negative potentials. The pH of the electrolyte solution was measured before and after each experiment without any changes.

2.2.3. Electrochemical impedance

Electrochemical impedance experiments were performed on the three different oxide film electrodes. In all cases, the stabilization of the electrode open circuit potential (OCP) was previously recorded until a minimal variation (ca. ±1 mV) was observed. Then the electrode was polarized to a selected potential as long as it was necessary to reach an

almost constant current value (changes by ca. ±0.1 μA) for approximately 1 h. The impedance measurements were performed by applying a small amplitude sinusoidal potential perturbation (10 mV) superimposed on the d.c. potential using a ZANHER IM5D analyzer. The impedance measurements on the different types of electrodes were performed at $f = 80$ Hz because this value is placed in the constant capacity–frequency range and the experimental noise from the electric source is minimal, as was shown previously [1].

The impedance response of metallic substrate/oxide film/electrolyte systems can be associated with an equivalent electric circuit containing a capacity element C_T in parallel with a resistance element R_{ox} and in series with another resistance element R_s. Here, C_T represents the total capacity of the electrode, R_{ox} the oxide film resistance of the electrode, and R_s the solution resistance. The total electrochemical impedance as a function of the angular frequency ω for this $R_s(R_{ox}C_T)$ circuit is given by

$$Z_{(\omega)} = R_s + \frac{R_{ox}}{1 + {R_{ox}}^2 {C_T}^2 \omega^2} - j\frac{{R_{ox}}^2 C_T \omega}{1 + {R_{ox}}^2 {C_T}^2 \omega^2} = Z_{real} + jZ_{imag} \quad (1)$$

where ω is equal to $2\pi f$, and f the frequency of the sinusoidal potential wave. The terms Z_{real} and Z_{imag} are the real and imaginary components of the impedance, respectively. For high enough values of ω, ${R_{ox}}^2 {C_T}^2 \omega^2 \gg 1$ and then $Z_{imag} \approx 1/(C_T\omega)$, so that changes in the imaginary part of the impedance reflect the changes in the total capacity of the system C_T at a given frequency.

Total capacity measurements (C_T) were performed between −0.8 and 1.5 V with a delay time of 10 s between successive applied potentials ($\Delta V = 0.05$ V) at different solution pH.

2.2.4. Photoelectrochemical measurements

The photoelectrochemical experiments were performed using an EG&G PAR Potentiostat/Galvanostat Model 263 connected to a computer through an IEEE 488 interface and two different illumination setups were employed: white or monochromatic light. A 150 W xenon lamp (Ushio) equipped with a water filter set was employed as excitation source. The photocurrent vs. excitation wavelength response was obtained using a monochromator SID 101 with a stepper motor assembly and an UD-5011 interface card and software, from Photon Technology International (PTI). The absolute intensity of the light coming from the monochromator was measured with a radiometer–photometer from Motorola. The intensity of the anodic photocurrent from the working electrode was detected by means of a two-phase lock-in amplifier EG&G PAR Model 5210 as a function of incident wavelength and applied electrode potential. The photocurrent spectra from the electrode were obtained using chopped light (15 or 80 Hz) and the chopper signal was fed to the reference channel of the lock-in analyzer. All the photoelectrochemical experiments were carried out in a cell with about 30 ml of solution equipped with a plane quartz window.

2.2.4.1. Potentiodynamic photoelectrochemical measurements performed at constant wavelength in a potential range from −0.2 to 1 V. Photocurrent–potential curves were recorded at 20 mV/s from −0.2 to 1 V in 0.1 M NaCl solutions. During the potential sweep, the electrode was illuminated with monochromatic or white light. The light was chopped at 15 Hz and the output from the potentiostat was directly recorded without amplification. The measured photocurrent values were almost independent of the potential scan direction.

2.2.4.2. Photoelectrochemical measurements performed at constant potential in a wavelength range from 250 to 420 nm (supra-bandgap region). Photoelectrochemical experiments were performed on the three types of TiO_2 oxide film electrodes with different constant potential applied between 0 and 2.0 V in order to select the working conditions where the photocurrent becomes potential independent. At each selected potential, the electrode was irradiated in the 250–420 nm range through a wavelength scanning with 1 nm spectral resolution. This energy range corresponds to higher values than the energy gap between the valence and conduction bands for the TiO_2 oxide and will be called hereinafter the supra-bandgap region. The electrode illumination and the wavelength scanning were started after a constant dark current value was achieved. The time constant for signal integration (about 0.1 s) was selected at the wavelength of maximal photocurrent. The light was chopped at 80 Hz, and a signal from a photodiode was used as reference and sent to the lock-in amplifier reference channel. The output from the potentiostat was connected to the lock-in signal channel so that the in-phase photocurrent could be detected. From these measurements a potential was chosen where the photocurrent–λ curves reach almost similar values.

2.2.4.3. Photoelectrochemical measurements performed at constant potential in a wavelength range from 400 to 700 nm (sub-bandgap region). The procedure was the same as in the Section 2.2.4.2, but the wavelengths range between 400 and 700 nm and corresponds to values lower than the TiO_2 bandgap. Due to the too low photocurrents recorded, the time constant for signal integration was about 10 times higher than in the supra-bandgap region.

3. Results and discussion

3.1. Structural characteristics of TiO_2 films on the titanium substrate

The titanium oxidation state into the nanocrystalline oxide film was obtained by means of UPS analysis. UPS spectra were taken at regular periods of sputtering time between

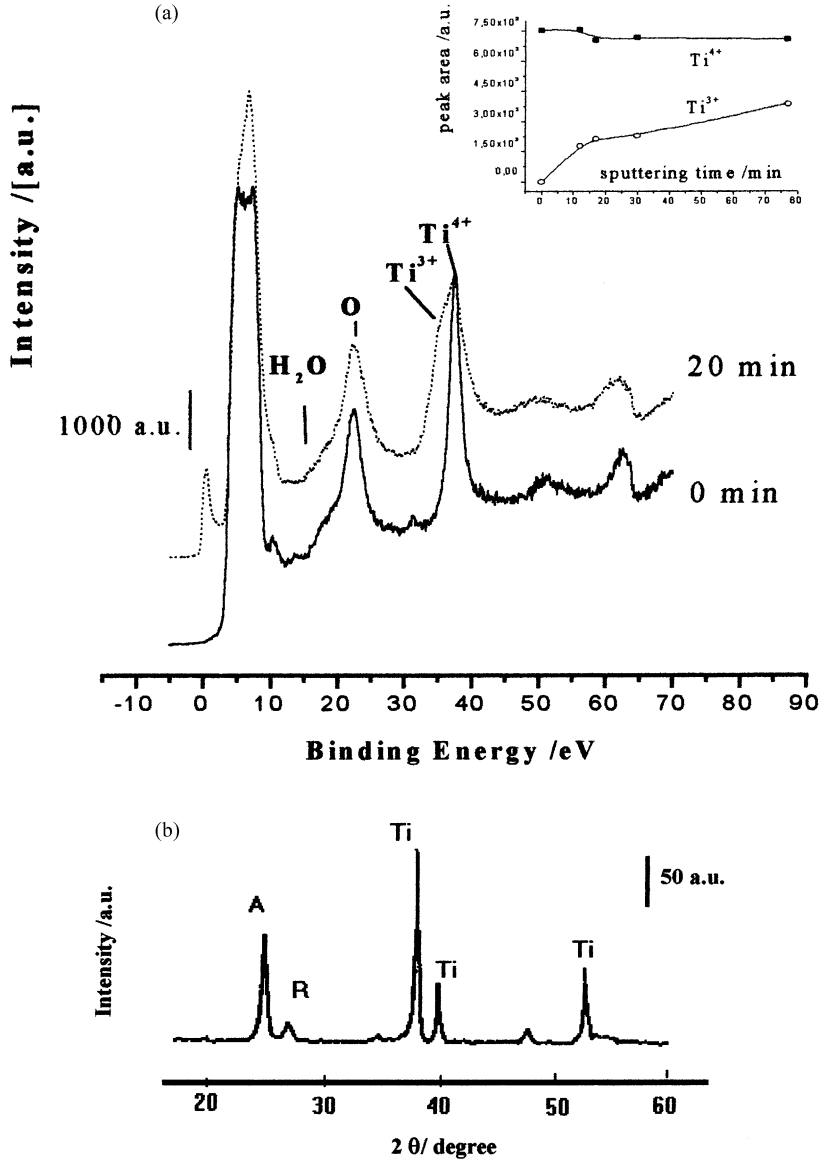

Fig. 1. (a) UPS spectra in arbitrary units at two different sputtering times (0 and 20 min) with argon ions (2 keV, 20 μA). The O 2s peak at 23 eV binding energy was taken as the reference signal. Inset: deconvoluted areas for Ti^{3+} and Ti^{4+} species as a function of sputtering time. (b) Experimental XRD of the nanocrystalline TiO_2 film sinterized at 400 °C. A represents the anatase phase, and R the rutile phase. Ti indicates signals coming from the metallic substrate.

0 and 2 h. Fig. 1a shows the UPS spectra at two different sputtering times at the binding energy E_b range where the signals corresponding to valence band energy, O 2s and Ti 3p, are expected to appear. The shape of the intensity profile related to the valence band (∼2–10 eV) changes with the sputtering time. The peak appearing in the 30–40 eV range reveals the presence of titanium atoms. The maximum in the spectra obtained without sputtering observed at 38.1 eV coincides with the binding energy value corresponding to the presence of the Ti(IV) oxidation state in the oxide film. After several minutes of sputtering, a shoulder appears at smaller values of E_b. From a deconvolution procedure of this peak, it is possible to obtain a second component at an energy value of 36.0 eV, indicating the presence of a lower oxidation state, probably Ti(III). This contribution becomes more significant for higher sputtering times (deeper oxide layers) as can be seen from the inset of the figure. These experimental facts may not be highly conclusive because a preferential sputtering of oxygen could produce the reduction of a small fraction of TiO_2. However, the changes observed on the calculated area for Ti(IV) and Ti(III) species for different deconvoluted spectra demonstrates that the Ti(III) species are not generated from Ti(IV). The presence of H_2O could be detected for all spectra obtained with and without sputtering. This bound water layer demonstrates the porous nature of the film that allows water molecules to reach the substrate. It is important to note here that the TiO_2 nanocrystalline film was deposited onto a titanium

substrate, which presents a spontaneously formed thin oxide layer with n-type semiconductor characteristics. The n-type semiconductor behavior of the nanocrystalline oxide film is determined by the presence of Ti(III) species. This experimental fact is opposite to the behavior observed by other authors in colloidal films [2]. This difference in semiconducting behavior can be attributed to the different precursors used in the electrode preparation by these authors.

The XRD spectrum for a nanocrystalline TiO_2 film is shown in Fig. 1b. The presence of an intense peak at 24.74 2θ degree indicates a predominant anatase crystalline structure. However, a small signal corresponding to the rutile phase (26.76 2θ degree) is also observed. The metallic titanium lattice from the substrate produces several intense signals as indicated in the figure.

3.2. Photoelectrochemical characteristics of TiO_2 films on the titanium substrate

3.2.1. Electrochemical characteristics

Fig. 2 shows voltammetric curves obtained in the dark for nanocrystalline Ti/TiO_2 electrodes in 0.1 M NaCl pH 4.7. The electrochemical behavior of thermally and electrochemically formed oxides is also included for comparison. The highly exposed surface area of nanocrystalline TiO_2 film produces higher current values in the potential range between −0.5 and −1.0 V than the thermal and electrochemical oxides. The current of the nanocrystalline electrode is approximately 30 times higher than that corresponding to the other two electrodes. However, this enhancement is not directly correlated to the roughness factor of 450 obtained from SEM. It indicates that the whole area of the nanocrystalline oxide film is not electrochemically active. The very small current profile observed at anodic potentials than −0.25 V is characteristic of a passive film on the substrate, which is a common feature of these three types of electrodes. The effect of H^+ concentration on the voltammetric curves for nanocrystalline Ti/TiO_2 electrodes (pH 3.5 and 9.0) can be observed in Fig. 3. The voltammograms obtained at pH 3.5 show a charge transfer process with a cathodic peak at −0.66 V and a complementary anodic peak at −0.53 V, these processes are not observed at higher pH. According to previous results [7], the peak appearing during the negative potential sweep corresponds to the reduction of Ti(IV) (hydr)oxide species at the surface in contact with the electrolyte and is related to the oxidation

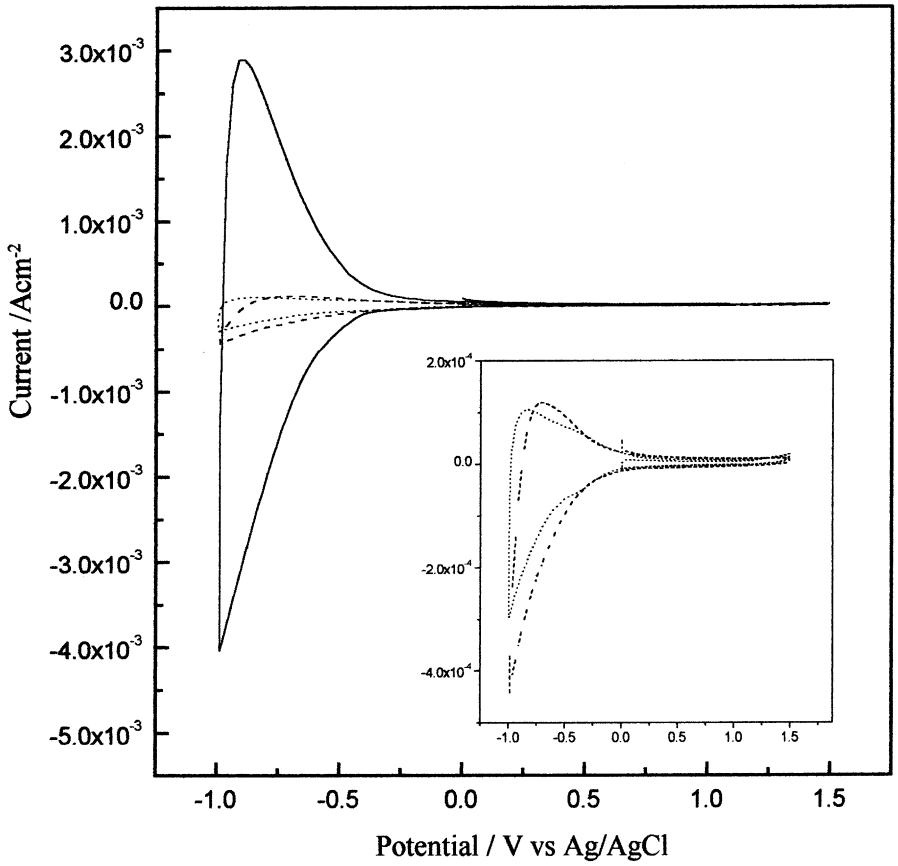

Fig. 2. Voltammetric curves obtained in the dark for nanocrystalline (solid line), thermal (dashed line) and electrochemical (dotted line) TiO_2 oxide film electrodes in 0.1 M NaCl, pH 4.7, at 100 mV s^{-1} potential sweep rate. The current density was calculated using the electrode geometric area. Inset: voltammetric curves for a thermal (dashed line) and electrochemical oxide (dotted line) electrode in the same potential range with a more sensitive current scale.

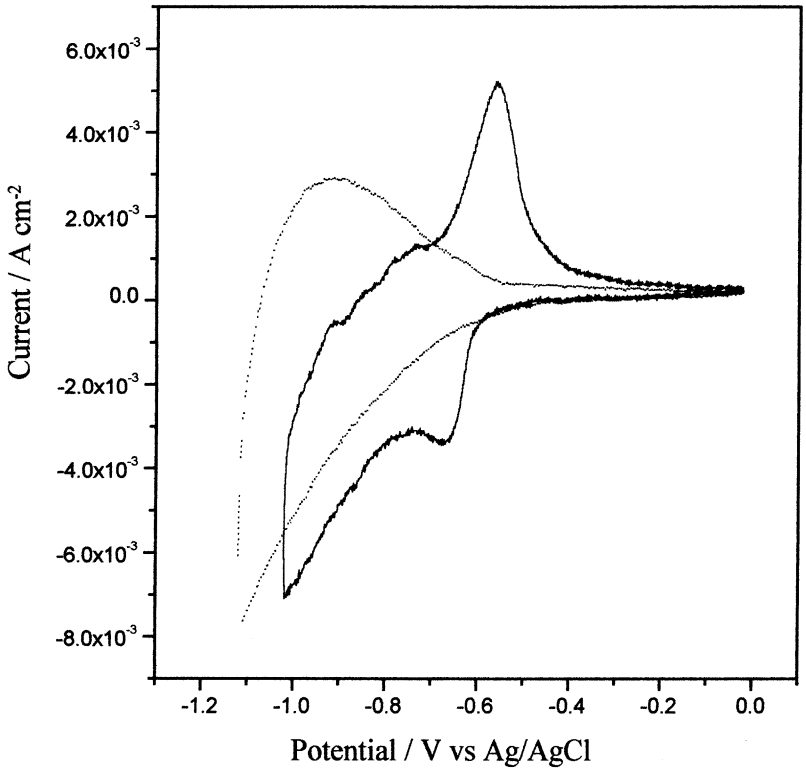

Fig. 3. Voltammetric curves obtained in the dark for a nanocrystalline Ti/TiO_2 electrode in 0.1 M NaCl at different pH values: 3.5 (solid line), and 9.0 (dotted line) at 10 mV s^{-1} potential sweep rate.

process of Ti(III) (hydr)oxide species obtained during the positive potential scan. This redox process could be expressed through the following chemical equation:

$$\succ Ti(OH)_2 + H^+_{(aq)} \leftrightarrow [\succ Ti(OH)(H_2O)]^+ + e^- \leftrightarrow \succ Ti(OH) + H_2O \quad (2)$$

The strong dependence of the *i–V* profiles with the solution pH shown in Fig. 3 is in accordance with the H^+ ions coming from solution which participate in Eq. (2).

From H^+ adsorption–desorption studies on TiO_2 colloidal suspensions [8], the relationship between H^+ concentration in solution and the surface charge developed due to the H^+ ions adsorption at the colloidal particle is well known. The fact that the nanocrystalline TiO_2 films present a high H^+ adsorption (indicated by the high current values of the observed cathodic–anodic couple at acidic pH values) has allowed the study of the adsorption–desorption process of other more complex species and its competitive behavior as a function of solution pH [1,9].

Fig. 4 shows capacity vs. potential curves under dark conditions for the three TiO_2 oxides in 0.1 M NaCl at pH 4.7. The corresponding Mott–Schottky plots [10] are shown in the inset. A passive oxide layer is always present at the surface of the titanium substrate, and it grows further under heat treatment. Because the TiO_2 film electrodeposited on the titanium plate is sintered at 400 °C, it is important to compare its behavior with that where the film is obtained by heating the titanium plate for the same time and under the same conditions as the electrodeposited sintered nanocrystalline film electrode. From the Mott–Schottky plots, donor concentration (N_D) and flat band potential (V_{FB}) were calculated and the values are shown in Table 1. It can be seen that the N_D values obtained for the three electrodes have the same order of magnitude. The V_{FB} are similar for the nanocrystalline and thermal TiO_2 oxide films, but the electrochemical oxide presents a more negative value. The similarity in V_{FB} could be due to the fact that both electrodes were heat-treated during their final preparation stage, reaching the same hydration degree at the surface oxide film. The interpretation of capacitance response carried out by Grätzel and co-workers [2] about colloidal TiO_2 particles spread on a titanium sheet establishes that the capacitance of the whole film under reverse bias is determined by the compact layer alone where a depletion layer is formed. Nevertheless, in our case, it was found that the capacitance response is

Table 1
V_{FB} values obtained from capacitance measurements at pH = 4.7

Type of film	V_{FB} (V)	N_D (cm^{-3})
Thermal oxide	−0.12	8.36×10^{19}
Electrochemical oxide	−0.76	3.10×10^{20}
Nanocrystalline oxide	−0.14	1.60×10^{20}

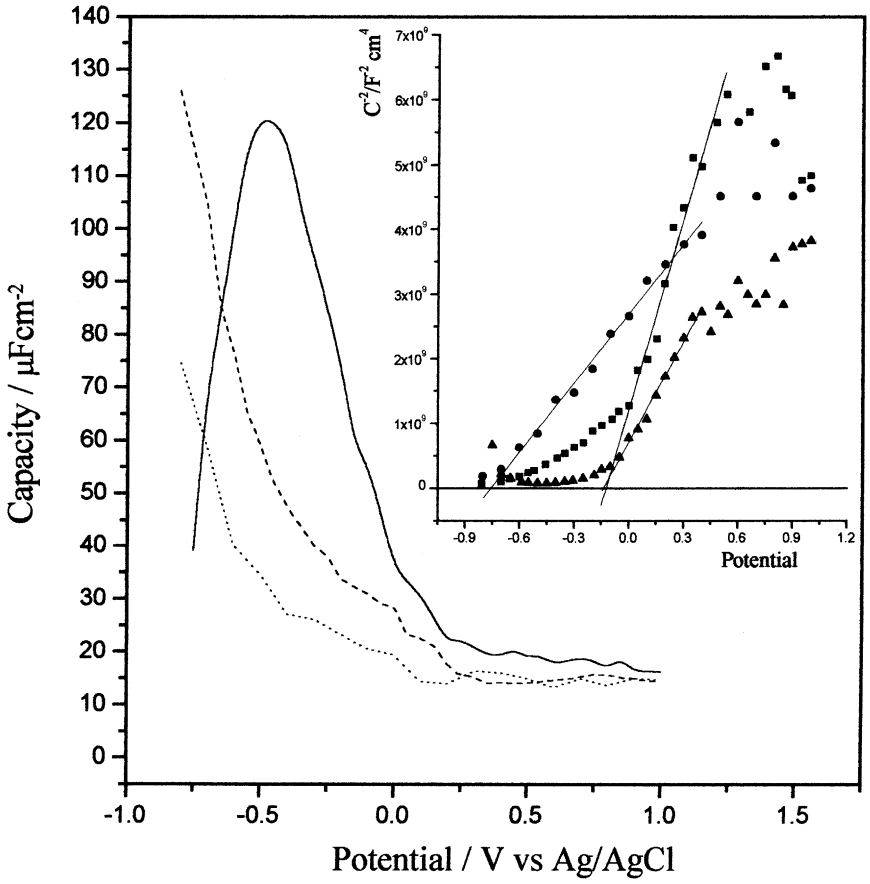

Fig. 4. Capacity–potential curves obtained at 80 Hz in 0.1 M NaCl, pH 4.7, in the dark, on a nanocrystalline (solid line), thermal (dashed-dotted line) and electrochemical (dotted line) TiO_2 electrodes. Inset: C^{-2}–V diagram (Mott–Schottky plot) for nanocrystalline (solid triangle), thermal (solid square) and electrochemical TiO_2 (solid circle) electrodes.

mainly determined by the electrodeposited film. This may be due to the presence of Ti(III) species in these films as it was determined by UPS analysis (Fig. 1a). Therefore, and according to Fig. 4, it can be expected that the capacitance response reflects the impedance of the large area of the n-type semiconductor film. The observed capacitance increases markedly by electrodepositing the nanocrystalline film on the titanium plate. Hence, the measured total capacity is dominated by the electrodeposited film in agreement with expectations. This result is opposite to that of Grätzel and co-workers [2] mainly because of the nature of the deposited film. In their case, the TiO_2 particulate film behaves nearly as an intrinsic semiconductor.

3.2.2. Different physical models to analyze the photocurrent–wavelength and potential dependence

We will give a brief theoretical introduction of photocurrent dependence on wavelength and electrode potential according to well-established physical models, and then a quantitative interpretation of the experimentally observed wavelength and potential behavior for the different electrodes will be carried out.

The dependence of the photocurrent spectra with the incident light energy was analyzed taking into account two physical models for light absorption: crystalline [10] or amorphous [11] semiconductors. The reason is that it is not possible to explain adequately the photoresponse in the whole wavelength range of these films within the theoretical framework of only one model.

As it was determined above, the nanocrystalline films present anatase phase, and so well-developed periodicity can be expected normal to the surface. The application of band structure models based on crystalline semiconductors seems to be appropriate also for amorphous films where a short range order exists. In the case of crystalline materials, the density of states at the border of the band decrease abruptly to zero, while amorphous semiconductors usually present an extensive tailing of electronic states into the bandgap. In this case, the energy value at which the photocurrent begins to be evident is called the mobility gap (E_g^{opt}) and is no longer a material constant but is dependent on oxide preparation methodologies.

The Gärtner–Butler equation [12,13] relates the photocurrent i_{ph} with the absorption coefficient α through the

following equation

$$i_{ph} = eJ_0\left(1 - \frac{e^{-\alpha W}}{1+\alpha L_p}\right) \quad (3)$$

where W is the thickness of the space charge layer in the semiconductor and L_p the minority carriers diffusion length. Taking into account that the quantum efficiency is given by $\Phi = i_{ph}/eJ_0$, where J_0 is the photon flux and e the electron charge, a direct proportional relationship between the quantum efficiency Φ and the absorption coefficient α in the whole spectral range can be obtained. To obtain this relationship, $\alpha W \ll 1$ and $\alpha L_p \ll 1$ should be fulfilled, so that the exponential in the Gärtner–Butler equation can be expanded in series. In this case, the photocurrent generation is directly proportional to the fraction of light absorbed in the space charge region W. Then, the behavior of light absorption by a crystalline semiconductor close to the absorption edge can be described with the i_{ph} being proportional to α through the relationship:

$$i_{ph} = A\frac{(h\nu - E_g)^n}{h\nu} \quad (4)$$

where $n = 0.5$ for direct optical transitions and $n = 2$ for indirect optical transitions, A is a constant which depends on the optical transition type and E_g the bandgap energy.

The restrictions applied to the Gärtner–Butler equation are verified under all experimental conditions since the light absorption coefficient α for TiO_2 lies typically in the range 1×10^2–$1 \times 10^4\,cm^{-1}$ for photon energies in the 3.0–3.6 eV range, i.e. near the energy of bandgap [14] and W typically lies in the 10–100 nm range for a crystalline n-type semiconductor with a donor concentration of $\sim 10^{20}\,cm^{-3}$ with a potential drop in the space charge layer of around 1 V.

In the case of amorphous semiconductors, an empirically observed phenomenon for energies near the band edge is, the so-called Urbach tail [15], described by the following equation

$$\alpha = a\exp\left[\frac{b(h\nu - E_g^{opt})^n}{kT}\right] \quad (5)$$

in which a and b are adjustable parameters. Several approximations for the i_{ph} vs. wavelength relationship were considered by different authors [16–18] and estimations of the optical bandgaps were made. It was determined that one of the most important causes concerning the magnitude obtained for E_g values was the oxide crystal structure and morphology. According to Eqs. (4) and (5), plots for various power laws should reveal information about how far from the expected ideal is the experimentally determined behavior of the system under study.

The potential dependence of the photocurrent has also different behavior, whether it comes from crystalline or amorphous semiconductors. For crystalline semiconductors, under certain limitations, such as not too high absorption coefficients and not too high band bending as mentioned before, the photocurrent can be expressed by

$$i_{ph}^2 = \left(\frac{2\varepsilon\varepsilon_0 I^2\alpha}{N}\right)(V - V_{FB}) \quad (6)$$

Other models include the effect of surface states or recombination processes which can influence the potential dependence of the photocurrent. Di Quarto et al. [19] have interpreted the curves of photocurrent as a function of applied potential for an anodic titanium oxide taking into account the recombination in the Onsager theory [20] which was previously developed for electrolytic solutions and then applied to amorphous materials by Pai and Enck [21]. These authors [19] derived a mathematical expression for the photogeneration efficiency of electron–hole pairs in solids, taking into account the photocurrent dependence on the potential at different photon energies.

3.2.3. Experimental dependence of the photocurrent with wavelength

Fig. 5a shows the raw photocurrent vs. wavelength spectra (without any correction for the photon emission of the light source) for nanocrystalline TiO_2 electrodes at different applied anodic potentials in 0.1 M NaCl at pH 4.7 in the complete wavelength range (supra- and sub-bandgap region). The dependence of the maximum in supra-bandgap photocurrent on the applied potential is shown in the inset. It can be observed that a saturation in the maximum of photocurrent is achieved at more anodic potentials greater than 1.5 V. Thus, a polarization of 1.5 V was selected as a working condition in order to compare the photoresponse in the supra-bandgap region of the three types of oxide film electrodes, which is shown in Fig. 5b. It can be seen that the photocurrents generated by the nanocrystalline Ti/TiO_2 electrode is greater than the photocurrent generated by the electrochemical and thermal ones, and that the absorption sets in at ~400 nm for the nanocrystalline and thermal oxides whereas the electrochemical oxide sets in at ~365 nm. From these i_{ph} vs. λ curves at the absorption edge for the three oxide film an analysis using Eq. (4) has been made in order to obtain the E_g corresponding to direct and indirect transitions. The values of E_g were estimated from extrapolation of the linear zone of $(h\nu i_{ph})^{1/n}$ vs. $h\nu$ plots for the three electrodes at different pH values considering both types of transitions, i.e., direct $(1/n = 2)$ and indirect $(1/n = 0.5)$.

Fig. 6 shows as an example the representations of the data at pH 4.7, and Table 2 the obtained E_g values for all the cases. Both representations present an energy region of linear behavior. These results prove that E_g is slightly pH dependent and, as expected, it is dependent on the preparative conditions of the oxide. The obtained E_g values for nanocrystalline Ti/TiO_2 electrode considering an indirect transition (process that is mainly found in poly- and mono-crystalline TiO_2) are lower than those reported in the literature (~3.2 eV) [16]. This effect could be explained taking into account that certain amorphous characteristics in the oxide film remain

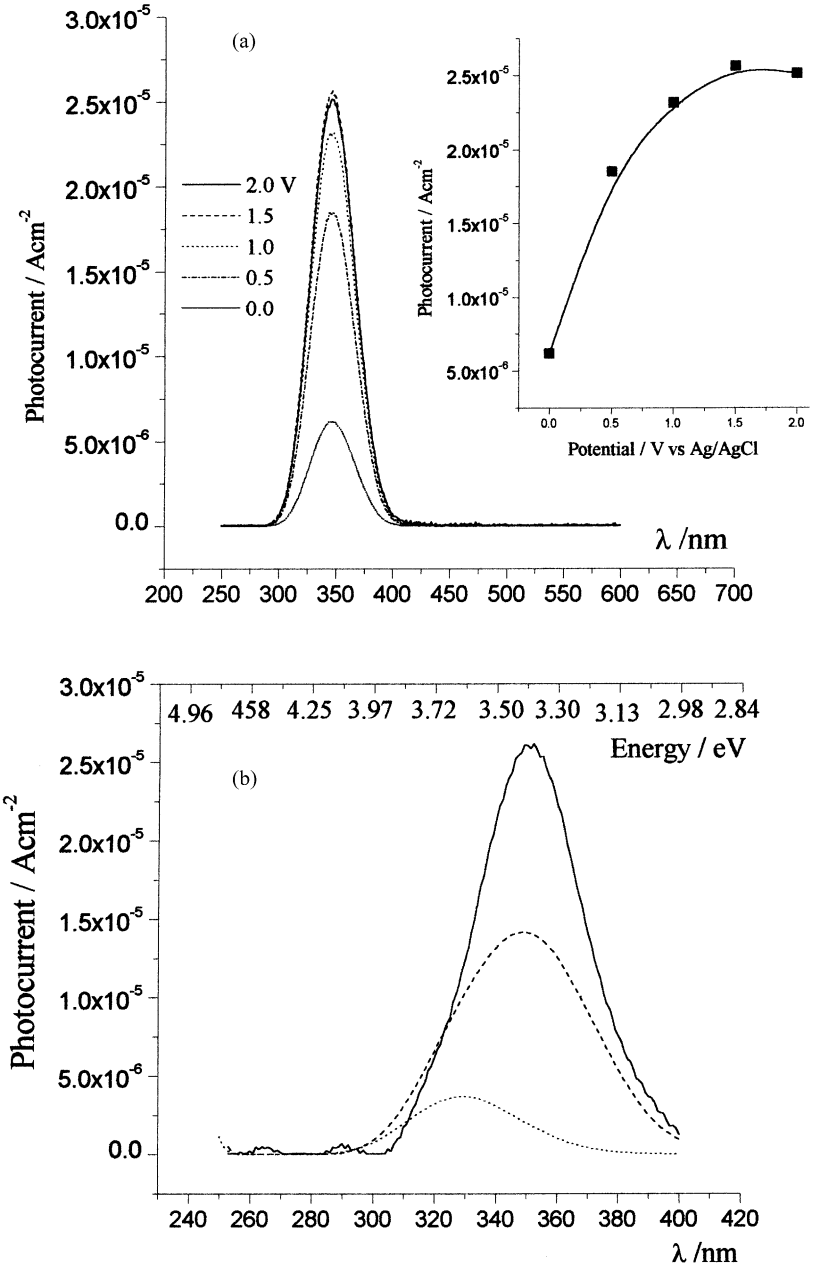

Fig. 5. (a) Raw photocurrent spectrum (without any correction for the photon emission of the light source) for a nanocrystalline TiO_2 oxide electrode in 0.1 M NaCl, pH 4.7; at different applied potentials in the whole wavelength range. Inset: photocurrent maximum values as a function of the applied potential. (b) Raw photocurrent spectrum (without any correction for the photon emission of the light source) for nanocrystalline (solid line), thermal (dashed line) and electrochemical (dotted line) TiO_2 electrodes in the same solution and pH as before at 1.5 V in the supra-bandgap region. The chopped light frequency was 80 Hz.

after the low temperature treatment (400 °C) in the synthesis of the nanocrystalline film. The E_g values obtained considering a direct transition would also be low compared with the values reported by other authors [22] (where 3.7 eV was obtained by an electron reflection technique). According to Halley et al. [17] and on the basis of their theoretical calculations performed for oxides anodically grown on titanium metal, there are several possible transitions between the valence and conduction bands at special points of the Brillouin zone which do not account for the bandgap energy. They found a dependence of the photocurrent–$h\nu$ plots with the film thickness and suggested that spectral characteristics observed in the near absorption edge are not associated with oxygen vacancies. Similarly, we found that the photocurrent curves depend on film thickness and applied potential for nanocrystalline electrodes which is analyzed in Fig. 7.

Fig. 7 shows the raw photocurrent vs. wavelength spectra for nanocrystalline Ti/TiO_2 electrodes prepared with

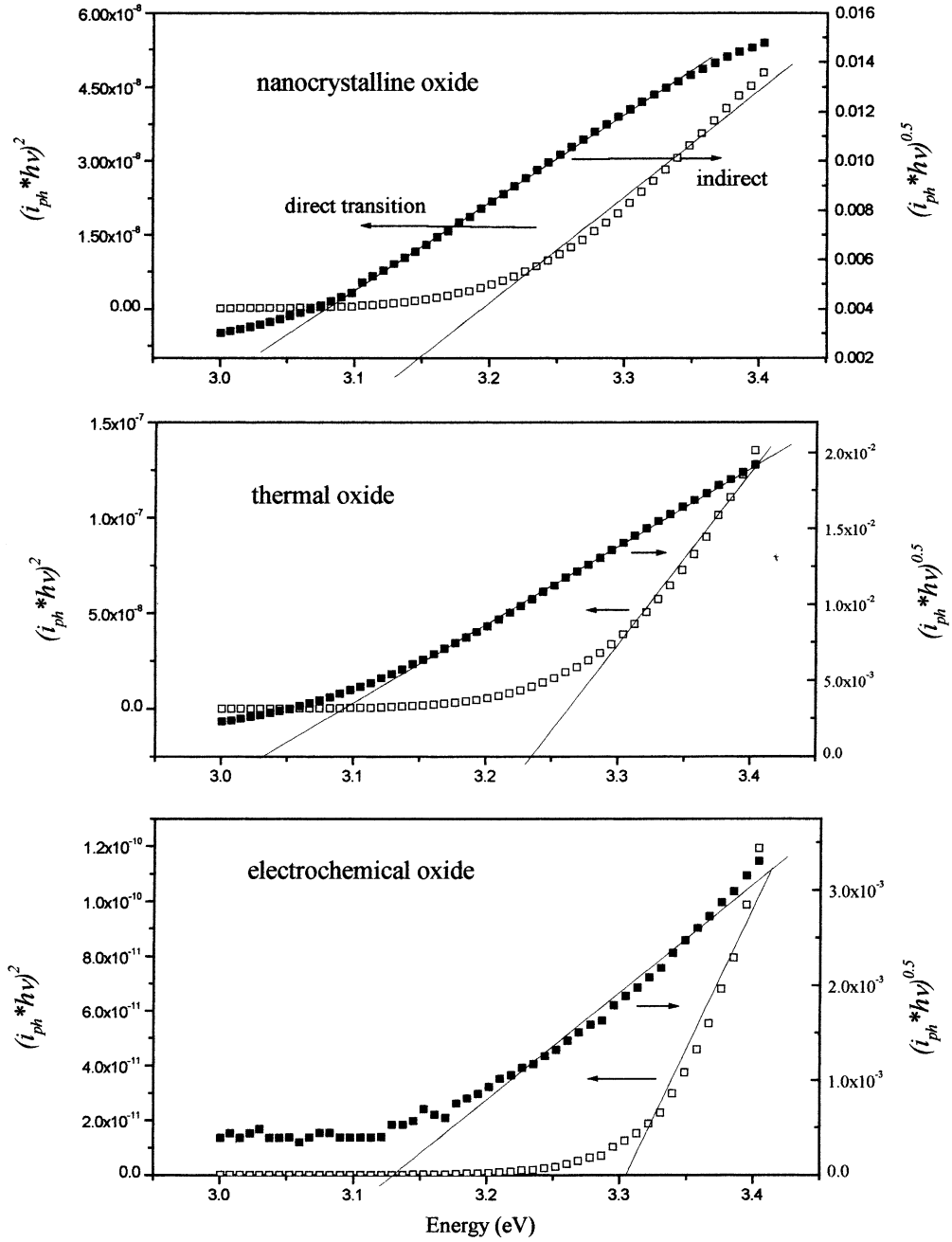

Fig. 6. Plots of $(i_{ph}h\nu)^{1/2}$ and $(i_{ph}h\nu)^2$ vs. $h\nu$ in a narrow energy range for the different oxide films obtained at pH 4.7. The calculated E_g values from these plots are shown at pH 3.3 and 4.7 in Table 2.

Table 2
E_g values derived from the interpolation of photocharacteristics vs. energy (Fig. 6) for different electrodes using Eq. (4) for interband transitions

Type of film	$1/n = 2$ (direct transition)		$1/n = 0.5$ (indirect transition)	
	pH 4.7	pH 3.3	pH 4.7	pH 3.3
Thermal oxide	3.26	3.19	3.03	2.92
Electrochemical oxide	3.31	3.29	3.13	3.10
Nanocrystalline oxide	3.19	3.09	2.97	2.83

different electrodeposition steps in 0.1 M NaCl at pH 4.7 in the: (a) 250–400 (b) 400–700 nm ranges, at a constant applied electrode potential of 1.5 V. The spectrum corresponding to one deposited layer in the sub-bandgap region is not shown due to the low photocurrent values compared to the other layers. It is noticeable that there is an increase in the photocurrent with the number of electrodeposited layers. The nanocrystalline film prepared with 10 deposit layers presents a shift in the light absorption towards shorter wavelengths in the supra-bandgap region; whereas the

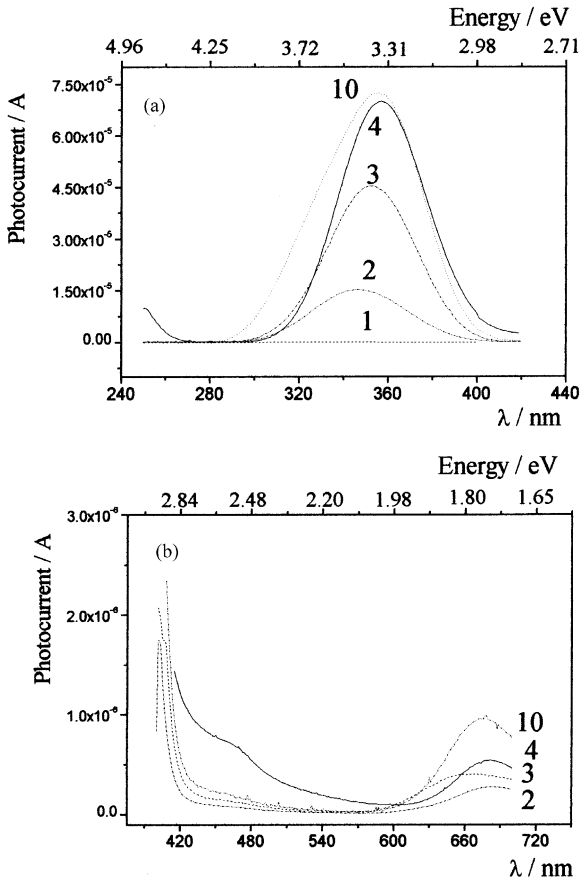

Fig. 7. Raw photocurrent spectrum (without any correction for the photon emission of the light source) for nanocrystalline TiO_2 oxide electrodes with different number of deposited layers (values included in the figure): (a) supra-bandgap region, and (b) sub-bandgap region. All the spectra were performed in 0.1 M NaCl, pH 4.7, at 1.5 V and the chopped light frequency was 80 Hz.

photocurrent between 600 and 700 nm presents the highest response. However in the 420–510 nm range, the higher response is given by the film prepared with four layers. Then the preparative procedure using four electrodeposition steps present the optimal response either at energies below or above the bandgap and it was chosen to perform the studies concerning adsorption and/or photodegradation processes [1,9].

Concerning the nanocrystalline electrode response in the region of the optical absorption edge, we suggest the determination of the *n* value by considering a different power law for the absorption edge region according to Eq. (5). Table 3 shows the optical bandgap E_g^{opt} thus obtained for nanocrystalline electrodes with different number of deposited oxide layers calculated from the fit of the optical absorption edge from the spectrum shown in Fig. 7. This fitting procedure was also applied for thermal and electrochemical oxides, and a value of approx. 1.0 for *n* was obtained, indicating a behavior associated with amorphous semiconductors according to [11]. The *n* values for nanocrystalline

Table 3
E_g^{opt} and *n* values deduced from a fit of the optical absorption edge using Eq. (5) for amorphous semiconductors

Number of electro-deposited layers	E_g^{opt} (eV)	*n*
1	3.60	1.25
2	3.12	1.27
3	3.15	1.30
4	3.00	1.50
10	3.01	1.98

electrodes tend to 2 as the number of deposited layers increases while it is observed that the optical bandgap for nanocrystalline oxide reaches almost 3.0 eV, as expected for indirect transitions (values are shown in Table 2). The *n* values may indicate that the behavior of these films is not exclusively due to a pure Urbach tail [15], but is more complex and cannot be approximated using Eq. (5). The overall decrease of E_g^{opt} for different deposited layers could be interpreted following the arguments developed by Mott and

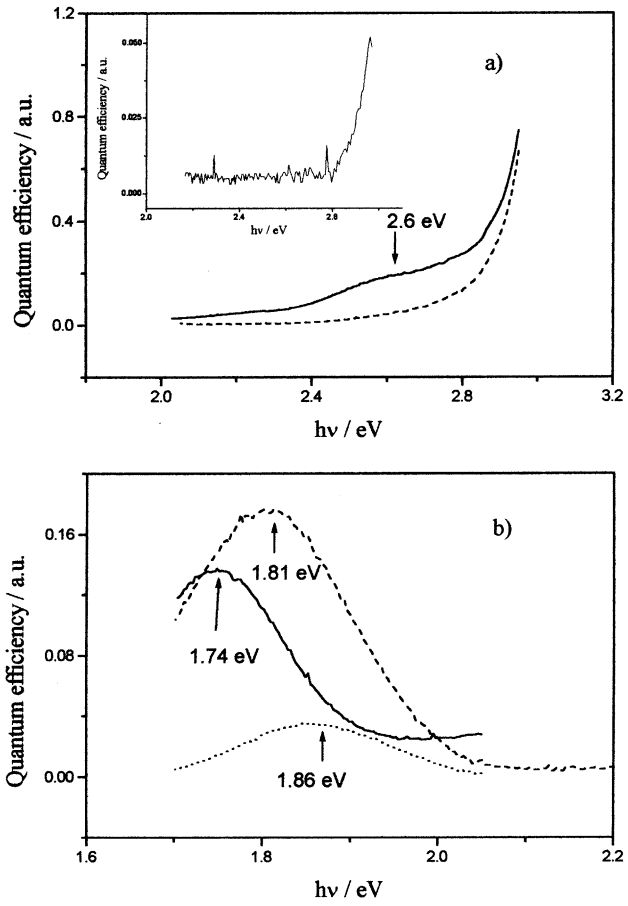

Fig. 8. Plots of the sub-bandgap quantum efficiency vs. incident photon energy for nanocrystalline (solid line), thermal (dashed line) and electrochemical (dotted line) TiO_2 oxide electrodes in 0.1 M NaCl, pH 4.7. The frequency of chopped light was 80 Hz. Photon energy range: (a) 2.0–3.0 eV; (b) 1.7–2.0 eV. The values indicated correspond to the energy for which the quantum efficiency is maximal.

Davis [11], according to which the changes in the bandgap energy reflect local order in the oxide material.

Now, we focus on the spectral region near the band edge and on the low-energy side near the photoresponse shoulder observed around 2.8 eV (∼425 nm) for nanocrystalline oxide film. Fig. 8a and b shows sub-bandgap quantum efficiency vs. incident photon energy for the three Ti/TiO_2 electrodes in 0.1 M NaCl, pH 4.7. The spectra were obtained in the potential range from 0 to 1.5 V. It was observed that the sub-bandgap photocurrent was essentially potential independent, and so only the spectrum obtained at 1.5 V is shown. These sub-bandgap spectra change drastically with the different electrodes. Only the spectra obtained for nanocrystalline electrodes present a shoulder at energies in the range 2.4–2.8 eV, to which a maximum of 2.6 eV was assigned from a deconvolution procedure. Possible origins of this shoulder are discussed below. In all cases, a peak below 2 eV (Fig. 8b) is detected with its maximum at different energies for the different oxide films. The position of the peak corresponding to the nanocrystalline oxide is more shifted towards lower energies and its quantum efficiency decreases significantly with respect to the other films.

Other authors [18,23] have reported a sub-bandgap photocurrent peak above 2 eV attributed to defect states that could be of a mixed nature, partly extrinsic and partly intrinsic. In our case, we also observed that the photocurrent in this range is sensitive to the state of the film, but not to the electrode applied potential. The range below 2 eV is insensitive to any of these parameters. It is noticeable that the peak below 2 eV always appears, independently of the titanium oxide formed. Indeed, the shoulder at ∼2.4–2.8 eV range was not found in thermal and/or electrochemical growth oxides. These facts could be indicating that the presence of the complex associated intrinsic–extrinsic defects should have more probability to be extrinsic in nature for the energies below 2 eV than at higher ones. Above 2 eV, the structures observed in the spectra should be related to the degree of order given by the crystalline lattice, and the defect levels

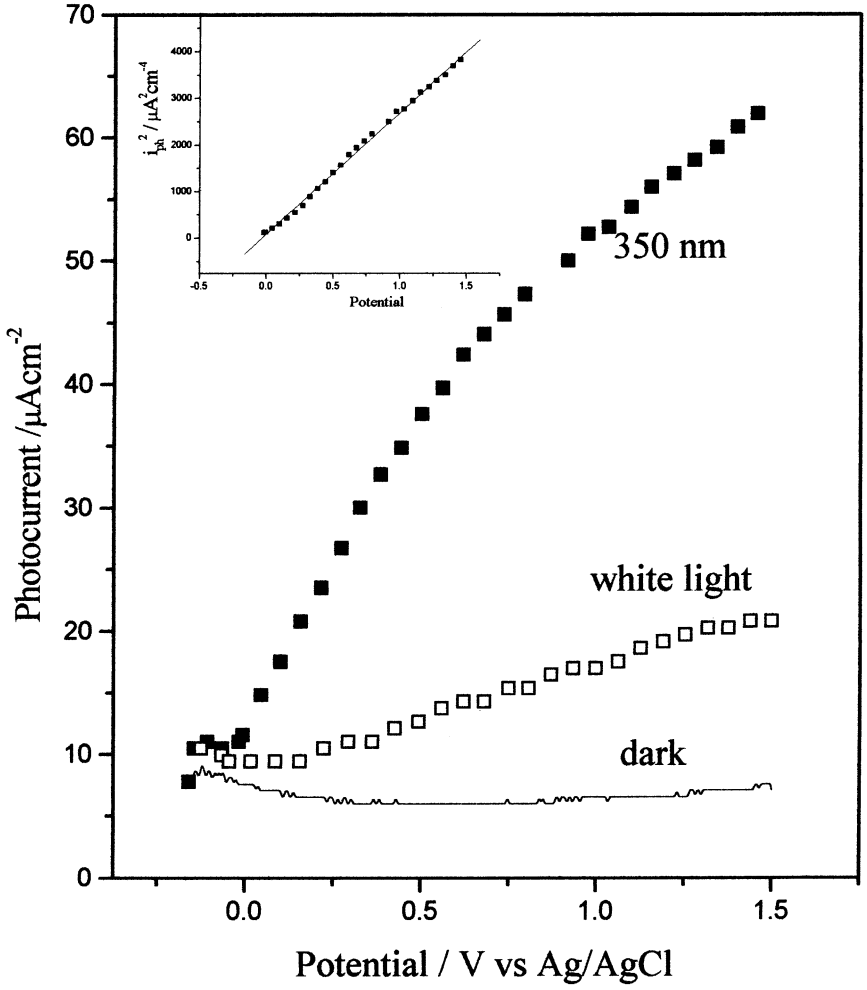

Fig. 9. Photocurrent–potential values obtained from the maximum in chopped (15 Hz) potentiodynamic curves (scan rate: 20 mV s^{-1}) for the nanocrystalline TiO_2 electrode irradiated with monochromatic light of 350 nm (solid square), white light (open square), and dark condition (solid line). Inset: plot of the photocurrent square (i_{ph}^2) vs. potential for a monochromatic light of 350 nm. The solid line shows the linear fit using Eq. (6).

Table 4
V_{FB} and α values obtained from i_{ph}^2 vs. potential plots for nanocrystalline electrodes at 350 nm and $\varepsilon = 173$

pH	V_{FB} (V)	α (cm^{-1})
3.3	−0.036	1.13×10^2
4.7	−0.187	1.025×10^2
9.6	−0.173	1.92×10^2

could be explained in terms of isolated defects, probably of intrinsic origin (oxygen vacancies, titanium interstitial and Ti(III) ions present in the n-TiO_2 lattice) according to the results presented in Fig. 7.

Below 2 eV, the existence of some intrinsic defect with an extrinsic impurity could account for the observed results (from Fig. 8). The nanocrystalline TiO_2 electrode that corresponds to the higher number of layers deposited gave the same values of photocurrent in this region, compared with the thermal oxide. Moreover, the peak maximum shifts toward energies matching with the ones corresponding to the thermal oxide. These defect levels could correspond to the same extrinsic impurity, making the photocurrent at ∼1.87 eV independent of the ordering.

3.2.4. Dependence of the photocurrent with the applied potential

Fig. 9 displays the photocurrent as a function of applied potential to the electrode, irradiated with white light and at a wavelength corresponding to the maximum observed in the photocurrent spectra ($\lambda \sim 350$ nm) chopped at 15 Hz. A higher photocurrent is observed when the electrode is illuminated at $\lambda \sim 350$ nm. The response obtained for anodic and thermal TiO_2 oxides was quite different (photocurrent squared vs. potential plots were not linear in the whole potential range) as it was also observed by other authors [19,22]. In the inset of Fig. 9 is shown the i_{ph}^2 vs. V dependence for nanocrystalline TiO_2 electrodes irradiated with 350 nm monochromatic light and the linear fit predicted by Eq. (6). From this type of representation, the V_{FB} and α parameters at different pH for nanocrystalline oxide films were calculated and are shown in Table 4. The dependence of V_{FB} with pH does not agree with the Nernstian relationship expected for almost all the oxide semiconductors, which was previously obtained for this type of electrode from capacitance measurements in electrochemical impedance experiments [24]. The α values do not change significantly with pH taking into account the experimental uncertainty in the data processing and the strong dependence (several orders in magnitude) with the incident energy informed for oxide films obtained by chemical vapor deposition techniques [25]. However, the same plot obtained for thermal and electrochemical oxides does not give a straight line (not shown here) which points to a more complex dependence. Concerning the Pool–Frenkel effect, a photocurrent vs. $V^{1/4}$ plots do not give a straight line in the whole range of potentials applied to the nanocrystalline electrode. However, it was possible to get a linear response in a narrow potential range for electrochemical formed oxides. Since this type of dependence is observed mainly for amorphous anodic oxides [26], its unfulfillment for nanocrystalline oxides could be due to the fact that this type of films have mainly crystalline structure. The photocurrent dependence on applied potential is determined principally by the behavior of a crystalline n-type semiconductor more than by the behavior corresponding to amorphous materials despite the fact that the energy defect levels inferred from photocurrent–wavelength curves.

4. Conclusions

The nanocrystalline oxide films have proved to have n-type semiconductor characteristics. The UPS analysis showed that the particulate TiO_2 film had Ti(III) species at very superficial layers and all throughout the film, conferring it a semiconductor behavior rather than an insulating one. From all the electrodes prepared, those obtained from nanocrystalline deposits showed the best photoresponse in the supra- and sub-bandgap regions. The analysis of different thickness showed an optimal value of four deposited layers concerning its photoresponse.

The experimental data obtained from chopped voltammograms and the results of theoretical simulations reported here confirm the crystalline character of the nanocrystalline films. However, the small amorphous degree could be associated to defect levels that respond to a Gaussian distribution in the sub-bandgap region. On the other hand, the fit performed for the electrochemical oxide suggests a higher disorder in the oxide lattice, with the thermal oxide having more local order than the electrochemical one despite the fact that no energy levels were present in the region between 2.0 and 3.0 eV.

Acknowledgements

Financial support from CONICET (Argentina) and SECYT (University of Córdoba) is gratefully acknowledged. The authors are indebted to the Alexander von Humboldt Foundation, World University Service (WUS), Centrum für Internationale Migration und Entwicklung (CIM) and Volkswagen-Stiftung for the donation of the equipments employed for the photoelectrochemical measurements. We are grateful to Lic. Walter Massad for lending us equipment to make photoelectrochemical measurements. We also want to acknowledge the LNLS (Brazil) for providing the TGM beamline and Dr. R. Landers and co-workers for helpful discussions and measurements assistance. The authors also thank Miss Pompeya Falcón for language assistance.

References

[1] F.Y. Oliva, L.B. Avalle, V.A. Macagno, C.P. De Pauli, Biophys. Chem. 91 (2001) 141.

[2] H. Anders, U. Björkstén, M. Grätzel, J. Phys. Chem. 100 (1996) 8045.
[3] L. Kavan, K. Kratochvilová, M. Grätzel, J. Electroanal. Chem. 394 (1995) 93.
[4] R. Hengerer, L. Kavan, P. Krtil, M. Gratzel, J. Electrochem. Soc. 147 (2000) 1467.
[5] H. Hidaka, K. Ajisaka, T. Oyama, K. Takeuchi, J. Zhao, N. Serpone, J. Photochem. Photobiol. A 138 (2001) 185.
[6] C. Natarajan, G. Nogami, J. Electrochem. Soc. 143 (1996) 1547.
[7] R.M. Torresi, O.R. Cámara, C.P. De Pauli, M.C. Giordano, An. Asoc. Quim. Argent. 74 (1986) 361.
[8] C. Giacomelli, M.J. Avena, C.P. De Pauli, Langmuir 11 (1995) 3483.
[9] F.Y. Oliva, L.B. Avalle, O.R. Cámara, in preparation.
[10] Yu.V. Pleskov, Yu.Ya. Gurevich, Semiconductor Photoelectrochemistry, Consultants Bureau, New York, 1986.
[11] N.F. Mott, E.A. Davis, Electronics Processes in Non-Crystalline Materials, 2nd Edition, Clarendon Press, Oxford, 1978.
[12] W.W. Gärtner, Phys. Rev. 116 (1959) 84.
[13] M.A. Butler, J. Appl. Phys. 48 (1977) 1914.
[14] D. Gorse, Modelling aqueous corrosion, in: K.R. Trehewey, P.R. Roberge (Eds.), NATO ASI Series E: Applied Science, Vol. 266, 1994, p. 337.
[15] F. Urbach, Phys. Rev. 92 (1953) 1324.
[16] K. Leiner, J.W. Schultze, U. Stimming, J. Electrochem. Soc. 133 (1986) 1561.
[17] W. Halley, M. Kozlowski, M. Michlewicz, W. Smyrl, N. Tit, Surf. Sci. 256 (1991) 397.
[18] J. Marsh, D. Gorse, Electrochim. Acta 43 (1998) 659.
[19] F. Di Quarto, S. Piazza, C. Sunseri, Electrochim. Acta 38 (1993) 29.
[20] L. Onsager, Phys. Rev. 54 (1938) 554.
[21] D.M. Pai, R.C. Enck, Phys. Rev. B 11 (1975) 5163.
[22] G. K Boschloo, A. Goossens, J. Schoonman, J. Electrochem. Soc. 144 (1997) 4.
[23] G. Nogami, S. Ohkubo, L. Avalle, K. Hongo, J. Electrochem. Soc. 143 (1996) 3600.
[24] F.Y. Oliva, Ph.D. Thesis, Facultad Ciencias Químicas, Universidad Nacional de Córdoba, Córdoba, Argentina, March 2001.
[25] K. Rajeshwar, J. Ibanez, in: Environmental Electrochemistry. Fundamentals and Applications in Pollution Abatement, Academic Press, New York, 1997, p. 545.
[26] S. Preusser, U. Stimming, S. Tokunaga, J. Electrochem. Soc. 142 (1995) 102.